

1 Possible patterns of marine primary productivity during the Great Ordovician 2 Biodiversification Event

3
4 Alexandre Pohl, David A.T. Harper, Yannick Donnadiou, Guillaume Le Hir, Elise
5 Nardin & Thomas Servais

6 Abstract

7 Following the appearance of numerous animal phyla during the ‘Cambrian Explosion’, the ‘Great
8 Ordovician Biodiversification Event’ (GOBE) records their rapid diversification at the lower taxonomic
9 levels, constituting the most significant rise in biodiversity in Earth’s history. Recent studies suggest
10 that the rapid rise in phytoplankton diversity observed at the Cambrian–Ordovician boundary may
11 have profoundly restructured marine trophic chains, paving the way for the subsequent flourishing
12 of plankton-feeding groups during the Ordovician. Unfortunately, the fossil record of plankton is
13 incomplete. Its smaller members represent the bulk of the modern marine biomass, but they are
14 usually not documented in Palaeozoic sediments, preventing any definitive assumption with regard
15 to an eventual correlation between biodiversity and biomass at that time. Here we use an up-to-date
16 ocean general circulation model with biogeochemical capabilities (MITgcm) to simulate the spatial
17 patterns of marine primary productivity throughout the Ordovician, and we compare the model
18 output with available palaeontological and sedimentological data.– 160/250 words –

19
20
21 Alexandre Pohl [pohl@cerege.fr], Aix Marseille Université, CNRS, IRD, Coll France, CEREGE, Aix-en-Provence,
22 France; David A.T. Harper [david.harper@durham.ac.uk], Palaeoecosystems Group, Department of Earth
23 Sciences, Durham University, Durham DH1 3LE, UK & Department of Geology, University of Lund, SE 223 62
24 Lund, Sweden; Yannick Donnadiou [donnadiou@cerege.fr], Aix Marseille Université , CNRS, IRD, Coll France,
25 CEREGE, Aix-en-Provence, France; Guillaume Le Hir [lehir@ipgp.fr], Institut de Physique du Globe de Paris,
26 Université Paris7-Denis Diderot, 1 rue Jussieu, Paris, France; Elise Nardin [elise.nardin@get.obs-mip.fr],
27 UMR5563 Géosciences Environnement Toulouse, Observatoire Midi-Pyrénées, CNRS, Toulouse, France;
28 Thomas Servais [thomas.servais@univ-lille1.fr], Univ. Lille, CNRS, UMR 8198 - Evo-Eco-Paleo, F-59000 Lille,
29 France.

30 Introduction

31

32 The 'Great Ordovician Biodiversification Event' (GOBE) was arguably the most important and
33 sustained increase of marine biodiversity in Earth's history (e.g. Sepkoski 1995; Webby 2004; Harper
34 2006). During the so-called 'Cambrian explosion' most, if not all, animal phyla first appeared in the
35 fossil record. Subsequently, during the Ordovician Period, an 'explosion' of diversity at the order,
36 family, genus, and species level occurred.

37

38 The search for the triggers of this biodiversification is ongoing, but most probably there was no
39 unique cause, but the combined effects of several geological and biological processes that helped
40 generate the GOBE.

41

42 During the Ordovician Period, a unique palaeogeographical scenario existed, with the greatest
43 continental dispersal of the Palaeozoic. High sea levels that were the highest during the Palaeozoic, if
44 not of the entire Phanerozoic, allowed marine waters to cover large epicontinental areas and flooded
45 large tropical shelf areas, enabling diversification (e.g. Servais *et al.* 2009, 2010). The climate was
46 warm, although recent studies indicate a significant, long cooling trend throughout the Ordovician,
47 followed up by an abrupt cooling at the end of the period, triggering the Late Ordovician glacial peak
48 (Trotter *et al.* 2008, Nardin *et al.* 2011, and Harper *et al.* 2014).

49

50 During the Ordovician, important ecological evolutionary changes occurred, beginning with the
51 'explosion' of the phyto- and zooplankton, leading to the 'Ordovician plankton revolution' (Servais *et al.*
52 2008). The onset of the GOBE is actually, at least partly for the planktonic groups, rooted in the
53 late Cambrian, when most of the planktonic organisms started to rapidly diversify (Servais *et al.*
54 2016). In this context, Saltzman *et al.* (2011) already considered that during the latest Cambrian a
55 major increase of atmospheric oxygen concentration (pO_2) had already taken place. The temporal
56 correlation between the Cambrian oxygenation event and the concomitant rise in plankton diversity
57 led Saltzman *et al.* (2011) and Servais *et al.* (2016) to hypothesize that the increase of pO_2 might have
58 triggered the increase of plankton diversity, which may be related to changes in macro- and
59 micronutrient abundances in increasingly oxic marine environments. The higher amount of available
60 nutrients in the oceans possibly triggered the development of pico- and phytoplankton, i.e. the basis
61 of modern marine trophic chains (Saltzman *et al.* 2011; Servais *et al.* 2016). Logically, the trophic
62 chain is then assembled with additional tiers provided by the suspension-feeding benthos (e.g.,
63 brachiopods, bryozoans and corals) and nekton, themselves prey to a range of predators, including
64 the trilobites, with orthoconic cephalopods and fishes at and near the top of the food chain.

65

66 Great advances have been made during the last decades concerning palaeogeographical

67 reconstructions for the Early Palaeozoic, including the Ordovician (e.g. Torsvik & Cocks 2013). These
68 more reliable global palaeogeographical reconstructions have allowed the formulation of simple
69 conceptual and more complex numerical models for ancient atmospheric and ocean circulation
70 patterns, or to hypothetically locate upwelling zones (e.g. Wilde, 1991; Christiansen & Stouge 1999;
71 Hermann *et al.* 2004; Pohl *et al.* 2014 ; Servais *et al.* 2014). More recently, new constraints on the
72 palaeobiogeography of marine living communities were provided by the publication of maps showing
73 much more precisely the ocean surface circulation modelled at various atmospheric CO₂ levels during
74 the Early, Middle and Late Ordovician (Pohl *et al.* 2016b).

75
76 The aim of the present paper is to model possible patterns of biomass production in the Ordovician
77 seas, in order to attempt to understand where and how the diversification originated. We use here
78 an ocean-atmosphere general circulation model with biogeochemical capabilities (MITgcm) in order
79 to simulate the changing spatial patterns of marine primary productivity in response to the
80 palaeogeographical evolution throughout the Ordovician. We subsequently attempt to compare the
81 model output with available palaeontological and sedimentological data.

82

83 **Ordovician biomass and the sedimentary record**

84

85 **Primary productivity in ancient oceans**

86 Many palaeontologists have focussed on the analyses of palaeobiodiversity during the Phanerozoic
87 (e.g., Sepkoski *et al.* 1981; Alroy 2010; Harper *et al.* 2015). Such studies lead to the understanding of
88 the major trends in biodiversification during Earth History, and to the discovery of the major
89 extinction phases, including the Big-Five mass extinctions. Specialists in macroevolution and
90 macroecology usually apply various statistical methods in order to better understand and interpret
91 the changing palaeobiodiversities (e.g. Sepkoski 1995; Bambach 2006; Alroy 2010; Stanley 2016). The
92 GOBE has also been recognized based on these studies.

93

94 Biodiversity is a measure of the number of biological organisms present at a given moment, but
95 usually provides no information about the abundance of these organisms. Little attention has been
96 paid to the evolution of the biomass in the oceans (e.g. Franck *et al.* 2006; Kallmeyer *et al.* 2012).
97 Similarly, the evolution of the abundance of nutrients available in the oceans during the history of
98 the Earth is only poorly known (e.g. Allmon & Martin 2014). In addition, biodiversity is not (at least
99 not directly) linked to the biomass produced (Irigoiien *et al.* 2004; Finnegan & Droser 2008). As a
100 result, little information is available about biomass, or the primary productivity in ancient oceans,

101 including that during the GOBE.

102

103 A few authors attempted to understand the evolution of the marine biomass during geological time.
104 Martin (2003), for instance, analysed the fossil record of biodiversity in relation to nutrients,
105 productivity and habitat area, whereas Martin *et al.* (2008) investigated the evolution of ocean
106 stoichiometry (nutrient content) in order to understand the biodiversification of the Phanerozoic
107 marine biosphere. Concerning the Ordovician, Payne & Finnegan (2006) considered that during the
108 GOBE the increase in the complexity of the marine trophic chains and in the efficiency of marine
109 organisms in removing available food, from both the water column and the sediment, appears to
110 account for a secular increase in animal biomass. Based on Martin *et al.* (2008), Servais *et al.* (2016)
111 further considered that the increasing presence of planktonic organisms in the late Cambrian – Early
112 Ordovician must coincide with increasing nutrient supply, increased primary productivity and
113 expanded biomass production, that resulted during the initiation of the GOBE with a higher diversity
114 and increased abundance of plankton-feeding groups during the Ordovician. Nowak *et al.* (2015)
115 effectively observed a dramatic increase in diversity of the acritarchs, i.e. the organic-walled fraction
116 of the phytoplankton, in the late Cambrian – Early Ordovician interval. But do the higher diversities
117 of phytoplanktonic organisms also indicate an increased abundance of phytoplankton, and an
118 increased biomass?

119

120 Ocean productivity largely refers to the production of organic matter by ‘phytoplankton’ (e.g. Sigman
121 & Hain 2012). In summary, most of the single-celled phytoplankton are ‘photoautotrophs’ that use
122 nutrients and light to convert inorganic to organic carbon. They are subsequently consumed by the
123 ‘heterotrophs,’ that include the ‘zooplankton,’ the ‘benthos,’ and the ‘nekton.’ The most important
124 nutrients necessary for the phytoplankton are nitrogen (N), phosphorus (P), iron (Fe), and silicon (Si),
125 while sunlight is the basic energy source needed. Until recently, it was assumed that the larger parts
126 of the phytoplankton (between 5 and 100 μm in diameter) account for most phytoplankton biomass
127 and productivity. This larger phytoplankton is partly preserved in the fossil record, and corresponds
128 in the Palaeozoic to the informal group of the acritarchs. However, recent studies indicate that more
129 than half of the biomass in modern oceans is actually produced by the much smaller fraction (< 2 μm
130 in diameter), referred to the picoplankton (e.g. Buitenhuis *et al.* 2012). Recent estimates indicate
131 that 30 % of the modern oceanic biomass is constituted by picoheterotrophs and 25 % of
132 picophytoplankton (e.g., Buitenhuis *et al.* 2013; Moriarty & O’Brien 2013). This small fraction is
133 almost entirely unknown from the fossil record, the picoplankton not being observed by
134 palaeopalynologists because it falls out of the range of classical observational methods. However,
135 most recent studies indicate that it is this fraction that is the most diverse in modern oceans (e.g., De

136 Vargas *et al.* 2015).

137

138 Thus, our understanding of the fossil record of the base of the trophic chain is highly incomplete in
139 the Ordovician, as only a minor fraction of the phytoplankton is recorded under the informal
140 grouping of, for example, the acritarchs. A key approach, therefore, to tentatively understand the
141 biomass production in the Early Palaeozoic is numerical models. In the present study we apply such a
142 model for three different time intervals in the Ordovician to tentatively understand marine
143 productivity during the GOBE interval. Our analysis specifically focuses on large-scale upwelling
144 systems, which generate high rates of biomass production and leave a distinctive fingerprint in the
145 sedimentary record.

146

147 Secondary production in upwelling systems

148 Modern coastal upwelling zones have been a focus of investigation for a number of years as loci of
149 bioproductivity. Here, benthic and nektonic diversity is influenced by a wide range of environmental
150 factors together with low-oxygen concentrations and biotic interactions such as competition and
151 predation. Upwelling zones promote bioproductivity through the delivery of nutrient-rich, deep
152 water onto the shelf, igniting the growth and abundance of phytoplankton. During the GOBE and
153 early stages of the establishment of the Palaeozoic Evolutionary Fauna, communities were
154 dominated by suspension feeders such as the brachiopods, bryozoans and corals and potentially
155 could benefit directly as primary consumers. There is a wealth of biodiversity data available for all
156 the major benthic and nektonic groups (e.g. Webby *et al.* 2004) but there are relatively few regional
157 studies related to specific geographic areas.

158

159 Recent studies of some of the key coastal upwelling zones, e.g. along the Namibian Coast (Eisenbrath
160 & Zettler 2016), associated with the Benguela Current Large Marine Ecosystem (BCLME), together
161 with those on coastal upwelling along the Peru coast (Rosenberg *et al.* 1983), the effects of El Nino
162 on the benthos of the Benguela, California and Humboldt upwelling ecosystems (Arntz *et al.* 2006)
163 and upwelling along the NW Africa coast (Thiel 1982) have established some key properties for these
164 zones. Primary and secondary production is substantial, however, it also generates low-oxygen
165 conditions commonly moving the Oxygen Minimum Zone (OMZ) into shallower-water environments.
166 Biotas are dominated by soft-bodied taxa, there is a reduced diversity and evenness and fewer
167 calcified forms (Levin 2003). In many cases assemblages are dominated by pioneer communities
168 populated by opportunistic species forming dense accumulations. Moreover, the poor oxygen
169 conditions encourage the migration of taxa into shallower water, extending too their geographic

170 ranges along the shelf. Organisms are abundant, generating substantial biomass but not necessarily
171 high diversities.

172

173 **Methods: model description**

174 **Ocean, atmosphere and sea ice**

175 We used a coupled ocean-atmosphere-sea ice setup of the Massachusetts Institute of Technology
176 general circulation model (MITgcm). An isomorphism between ocean and atmosphere dynamics is
177 exploited to allow a single hydrodynamical core to simulate both fluids (Marshall *et al.* 2004). The
178 oceanic and the atmospheric components also share the same cubed-sphere grid with 32 x 32 points
179 per face (cs32), yielding a mean equatorial resolution of 2.8° x 2.8°. The cubed-sphere grid avoids
180 polar singularities resulting from the convergence of the meridians at the poles, thus ensuring that
181 the model dynamics there is treated with as much fidelity as elsewhere (Adcroft *et al.* 2004).

182 The oceanic component is an up-to-date, hydrostatic, implicit free-surface, partial step topography
183 ocean general circulation model (Marshall *et al.* 1997*a, b*). Twenty-eight levels are defined vertically,
184 the thickness of which gradually increases from 10 m at the surface to 1300 m at the bottom. Effects
185 of mesoscale eddies are parameterised as an advective process (Gent & McWilliams 1990) and an
186 isopycnal diffusion (Redi 1982). The nonlocal K-Profile Parameterisation (KPP) scheme of Large *et al.*
187 (1994) accounts for vertical mixing in the ocean's surface boundary layer, and the interior. The
188 atmospheric physics is based on the Simplified Parameterisations, Primitive-Equation Dynamics
189 (SPEEDY) scheme (Molteni 2003). The latter comprises a four-band longwave radiation scheme, a
190 parameterisation of moist convection, diagnostic clouds, and a boundary layer scheme. A low vertical
191 resolution is used. Five levels are defined: one level represents the planetary boundary layer, three
192 layers are placed in the troposphere and the fifth layer is placed in the stratosphere. The pressure
193 coordinate p is employed. Sea ice is simulated using a thermodynamic sea-ice model based on the
194 Winton (2000) two and a half layer enthalpy-conserving scheme. Sea-ice growth occurs when the
195 ocean temperature falls below the salinity dependent freezing point.

196 Fluxes of momentum, freshwater, heat, and salt are exchanged every 20 minutes in the model (i.e.,
197 the ocean time step). The resulting coupled model can be integrated for ca. 100 years in one day of
198 dedicated computer time. Relatively similar model configurations were used in the past (Enderton &
199 Marshall 2009; Ferreira *et al.* 2010; 2011), including those for palaeoceanographical purposes
200 (Brunetti *et al.* 2015; Pohl *et al.* 2017).

201 **Primary productivity**

202 The MITgcm includes a biogeochemistry model that simulates the net primary productivity (NPP) in
203 the ocean. NPP is computed based on Michaelis-Menten equations as a function of available
204 photosynthetically active radiation (PAR) and phosphate concentration (PO_4),

$$205 \quad NPP = \alpha \frac{PAR}{PAR + K_{PAR}} \frac{PO_4}{PO_4 + K_{PO_4}}$$

206 where $\alpha = 2 \times 10^{-3} \text{ mol m}^{-3} \text{ yr}^{-1}$ is the maximum community productivity, $K_{PAR} = 30 \text{ W m}^{-2}$ the half
207 saturation light constant, and $K_{PO_4} = 5 \times 10^{-4} \text{ mol m}^{-3}$ the half saturation phosphate constant. In this
208 configuration, phosphate is the single limiting nutrient. It is consumed in the photic zone to fuel the
209 marine primary productivity, regenerated by remineralisation throughout the water column based
210 on the empirical law of Martin *et al.* (1987), redistributed within the ocean using the velocity and
211 diffusivity fields provided by the general circulation model and ultimately returned back to the ocean
212 surface in upwelling zones. Because phosphate is assumed to have an oceanic residence time much
213 longer than the oceanic turnover time scale (i.e., 10–40 kyr; Ruttenger 1993; Wallmann 2003), its
214 global oceanic concentration is fixed in the model (Dutkiewicz *et al.* 2005). Iron is known as another
215 major factor in productivity (Falkowski 2012). Because it is mainly delivered to the ocean surface as
216 dust from deserts, the emissions of which are difficult to quantify today (Bryant 2013); providing the
217 model with seasonal maps of iron input in the Ordovician is challenging. Although our
218 biogeochemical model has the provision to account for cycling of iron, we prefer not to consider iron
219 fertilisation here. The PAR is computed at the ocean surface as a fraction of the incident shortwave
220 radiation provided by the atmospheric component of the MITgcm. It is then attenuated throughout
221 the water column assuming a uniform extinction coefficient. Similar configurations of this
222 biogeochemistry model have been used in the past (Friis *et al.* 2006; 2007), including those for the
223 Ordovician (Pohl *et al.*, 2017).

224 **Boundary and initial conditions**

225 We ran our model on three palaeogeographical reconstructions representative of the Early
226 Ordovician (480 Ma, Tremadocian), the Middle Ordovician (460 Ma, Darriwilian) and the early
227 Silurian (440 Ma, Aeronian). The location of the continental masses is taken from the reconstructions
228 by Torsvik & Cocks (2009). The topography and the bathymetry are reconstructed based on
229 published global reconstructions, with additional information from regional studies for Gondwana
230 (e.g. Torsvik & Cocks 2013), Laurentia (e.g. Cocks & Torsvik 2011), Baltica (e.g. Cocks & Torsvik 2005),
231 Siberia (e.g. Cocks & Torsvik 2007) and Asia (e.g. Cocks & Torsvik 2013). Because the location and
232 depth of Ordovician ocean ridges is not well constrained, they are not included in the model. We use
233 a flat-bottom ocean, the depth of which is set to present-day mean seafloor depth, i.e., –4000 m

234 (Pohl *et al.* 2014). The flat bottom is not expected to constitute a major bias. Several studies on late
235 Palaeozoic oceans suggest that it does not critically impact the large-scale patterns of simulated
236 ocean circulation (Montenegro *et al.* 2011; Osen *et al.* 2012). The resulting palaeomaps are very
237 similar to those used by Pohl *et al.* (Pohl *et al.* 2016b).

238 A gradual greening of the continents occurred throughout the Ordovician. The first, non-vascular
239 land plants are documented from the Middle Ordovician Dapingian (Rubinstein *et al.* 2010). There is
240 no evidence of plants on land before that date, including during the Tremadocian, i.e., the first time
241 slice used in the present study. In addition, the spatial cover of this primitive vegetation is difficult to
242 estimate for the remainder of the period (Edwards *et al.* 2015; Porada *et al.* 2016). As a consequence
243 we here follow previous studies (Nardin *et al.* 2011; Pohl *et al.* 2014) and impose a rocky desert
244 landscape on the continents (ground albedo of 0.24, which is potentially modified by snow).

245 During the Ordovician, the atmospheric partial pressure of CO₂ ($p\text{CO}_2$) was significantly higher than
246 today (e.g. Berner 2006). However, the MITgcm does not account for varying $p\text{CO}_2$ levels. It is tuned
247 to the present-day $p\text{CO}_2$. We therefore increased the solar forcing in the model to simulate various
248 climatic states (Ferreira *et al.* 2011) and subsequently compared the simulated temperatures with
249 Ordovician estimates. A solar constant of 350 W m⁻² (instead of 342 W m⁻² today) induces an increase
250 in tropical sea-surface temperatures (SSTs) up to 32.5 °C to 33.7 °C (depending on the time slice
251 considered). These values compare well with the SSTs reconstructed by Trotter *et al.* (2008) for the
252 Middle Ordovician based on $\delta^{18}\text{O}$ measurements (see their Fig. 3 in particular). Alternative values
253 would better fit the Early and the Late Ordovician SSTs, but we here aim at quantifying the impact of
254 the palaeogeographical changes on the spatial patterns of Ordovician primary productivity, all other
255 things kept equal. We therefore conduct our three simulations using a solar constant of 350 W m⁻²,
256 which are here selected to provide the best match with Middle Ordovician SST estimates. The orbital
257 configuration is defined with an obliquity of 23.45° and an eccentricity of 0°.

258 We use identical initial conditions in all simulations, including an homogeneous salinity of 35 psu
259 (practical salinity units) and a theoretical latitudinal gradient of ocean temperature characterised by
260 equatorial and polar SSTs of respectively 35 °C and 6 °C and an ocean bottom potential temperature
261 of 3 °C. These values ensure that the ocean is sea ice free at the beginning of each model run.
262 Phosphate is initialised with its present-day depth profile. For each simulation, the physical ocean-
263 atmosphere-sea ice model is first run until deep-ocean equilibrium is reached (≥ 2000 model years).
264 It is subsequently restarted with marine biogeochemistry for 550 additional years and climatic fields
265 used for analysis are averaged over the last 50 years of the simulation.

266

267 **Results: simulated Ordovician marine productivity**

268 **In space: wind belts and Ekman pumping**

269 The main patterns of simulated Ordovician surface primary productivity (Fig. 1) reflect in simple
270 terms the ocean phosphate concentration, while the PAR only imposes a hemispheric-scale decrease
271 of NPP with latitude. The phosphate concentration in surface seawaters results, in turn, from the
272 large-scale patterns of Ekman pumping. The concentration in PO_4 is lower in shallow waters because
273 nutrients are consumed during photosynthesis and it increases with depth due to remineralisation of
274 sinking particles. Upwelling systems allow nutrient-rich deep waters to be transported back to the
275 surface and they are therefore associated with locally high phosphate content. On the contrary,
276 down welling areas are poor in nutrients. The spatial patterns of upwelling and down welling are
277 essentially driven by the direction of the wind blowing over the ocean surface through Ekman
278 pumping and suction. The Trade Winds induce large-scale upwelling systems on the western margin
279 of tropical landmasses, and the Westerlies cause high phosphate concentrations at the mid-latitudes
280 ($40^\circ - 60^\circ$). Between the Trade Winds and the Westerlies, the down welling of surface waters along
281 the tropics (30°) leads to low phosphate levels. A local minimum in phosphate concentration and
282 thus primary productivity occurs in the Palaeo-Tethys, between the eastern coasts of Baltica and the
283 western margin of tropical Gondwana (Fig. 1A-C). Here, the down welling of surface waters combines
284 with a strong freshwater input from the continent. The latter results from the intense orographic
285 precipitation that occurs when the moisture-laden Westerlies intercept the coastal topography of
286 Gondwana. Pohl *et al.* (2017) demonstrated that this strong runoff to the ocean is a robust model
287 result that it not overly model-dependent. While the polar latitudes ($60^\circ - 90^\circ$) are dynamically
288 isolated from the global ocean and thus depleted in phosphate in the Northern Hemisphere (Pohl *et*
289 *al.* 2017), deep-water convection along the coast of Gondwana (e.g. Poussart *et al.* 1999; Herrmann
290 *et al.* 2004) drives the local enrichment of surface waters in nutrients, ensuring relatively high
291 productivity levels there.

292 Although the small-scale spatial patterns of simulated NPP may be model-dependent to some extent,
293 the fact that the first-order signal results from a fundamental characteristic of Earth's climate (the
294 zonal wind belts) suggests that these results are relatively robust (Pohl *et al.*, 2017).

295 **In time: throughout the Ordovician**

296 The three studied time slices share a certain number of common features (Fig. 1). The western
297 margin of Laurentia, first, is associated with high levels of simulated NPP. In both hemispheres, the
298 mid-latitudes are further characterised by zonal currents inducing Ekman pumping and the upwelling

299 of nutrients fuelling a strong productivity. On the contrary, low marine productivity levels typify the
300 tropics (30°), the margin of Gondwana situated over the South Pole and the Northern high-latitudes.
301 A local minimum persists throughout the period at 30° S between the western coast of Gondwana
302 and the tropical landmasses.

303 Nevertheless, major changes can be observed from 480 Ma to 440 Ma (Fig. 1). The most considerable
304 alteration of the NPP patterns between the Early and the Late Ordovician resulted from the gradual
305 drift of Gondwana to the North. Confined in the Southern Hemisphere at 480 Ma, the supercontinent
306 reached 30° N at 440 Ma. The direct consequence of this continental drift was the appearance of a
307 major upwelling system at tropical latitudes in the Late Ordovician along the coasts of Gondwana
308 (Australia and India) and South China-Annamia. The contrast between the eastern and western
309 tropical coasts of Gondwana increased at the same time, with simulated NPP significantly decreasing
310 along the eastern coast of Gondwana at 440 Ma. Elsewhere, the spatial patterns of simulated NPP
311 remained relatively stable as the tropical continental masses slowly migrated to the North. This
312 continental drift prompted Siberia to slowly shift, from the Early to the Late Ordovician, from the
313 zone of minimum NPP reported previously at 30° S to the highly productive Panthalassic circumpolar
314 current. On the contrary, Baltica underwent a migration from nutrient-rich mid-latitude waters in the
315 Southern Hemisphere at 480 Ma to the depleted water masses centred on 30° S at 440 Ma.

316

317 **Discussion**

318 Here we compare our modelling results with the Ordovician geological record in order to validate our
319 simulations. We also discuss some enigmatic biotic events in the light of our model runs, such as the
320 sudden and widespread bioherm development that punctuated the Late Ordovician of Baltoscandia.

321 **Geological evidence for upwelling systems**

322 During the Ordovician two key coastal areas are typified by high levels of primary productivity in the
323 model: the west coasts of Laurentia and tropical Gondwana (Fig. 1), in particular Australia and South
324 China. These modelling results are supported by geological data. Indeed, a wide range of
325 sedimentary indicators has been confirmed for a prolonged phase of upwelling across much of
326 Laurentia during the Middle and Late Ordovician related to glaciation (Pope & Steffen 2003). A
327 careful reassessment of the ages of many of the units (Leslie & Bergström 2003) indicates that the
328 formation of cherts may be much more widespread, suggesting the possibility that this is related to
329 more general phases of upwelling across the Laurentian continent. Associated biotic indicators are
330 sparse and under-developed. Graptolites, however, were most common in upwelling zones along

331 continental margins. In the Vinini Formation, Roberts Mountains, Nevada, for example, changes
332 within the graptolite zooplankton have been associated with fluctuating oceanographic conditions
333 and the upwelling of anoxic waters. During high-stands graptolite faunas diversified within the OMZ
334 but the ecosystem collapsed with the substantial fall of sea level associated with the end Ordovician
335 glaciation and the retreat of the OMZ (Finney *et al.* 2007). Elsewhere in the Great Basin the macro-
336 shelly fauna is abundant throughout much of the Ordovician, forming locally shell beds and
337 concentrations (Finnegan & Droser 2005), with individuals increasing in size (Payne & Finnegan 2006)
338 and shell thickness (Pruss *et al.* 2010); the faunas are never highly diverse but they are abundant.
339 Bryozoan-rich deposits, formed by another suspension feeder, have also been associated with the
340 upwelling of nutrients in parts of Laurentia during the later Ordovician (Taylor & Sendino 2010).

341 In detail the location of the large-scale upwelling systems simulated in the model is in relatively good
342 agreement with most of the evidence of upwelling (cherts and phosphate deposits) documented by
343 Pope & Steffen (2003) (Fig. 1A). Best match is observed on the western margin of the tropical
344 landmasses, i.e., Laurentia and Gondwana. Some data points are more difficult to explain (e.g., in
345 southeastern Laurentia), and the most outstanding model-data mismatch is observed in Baltica.
346 Clearly, our simulation provides no explanation for the preservation of cherts in that precise location.
347 In order to explain the discrepancy, we emphasize that the spatial resolution of our model (ca. 300
348 km) does not allow us to capture small-scale processes. In addition, the land-sea mask interpolated
349 on the model's grid constitutes a crude approximation of Ordovician coastlines. Finally, current
350 palaeogeographical reconstructions only provide first-order indications of Early Palaeozoic
351 bathymetry and topography and they generate large uncertainties in the position of the continental
352 masses (up to 15° in latitude) (Lees *et al.* 2002), which makes any straightforward model-data
353 comparison challenging.

354 To explain the appearance of these unusual carbonates with abundant chert and phosphate, Pope &
355 Steffen (2003) required the strengthening of the meridional overturning circulation and associated
356 increased nutrient supply to the ocean surface in response to glacial onset during the late Middle
357 Ordovician. Because similarly high levels of primary productivity are simulated on the western
358 margin of Laurentia during each of the three studied time slices (Fig. 1A-C), with no ice sheet over
359 the South Pole, our model suggests that such coastal upwelling may instead have been a persistent
360 characteristic of Ordovician oceans. These results are supported by the reappraisal of the age of
361 many of the deposits originally reported by Pope & Steffen (2003), a number of them being
362 potentially Early Ordovician in age (Leslie & Bergström 2003). Together this raises serious doubts
363 about the climatic implications of the phosphatic rocks proposed by Pope & Steffen (2003). Glacial
364 onset does not seem to be a necessary condition for strong upwelling to occur along the margin of

365 Laurentia.

366 Another possible indicator of high levels of primary productivity is the preservation of sediments
367 enriched in organic matter. Melchin *et al.* (2013) published a compilation of Late Ordovician – early
368 Silurian black shale occurrence. They illustrated three time slices immediately before, during and
369 right after the Hirnantian glacial peak. Using simulations similar to ours, but focusing on the Late
370 Ordovician, Pohl *et al.* (2017) recently demonstrated a striking correlation between the regions of
371 high (low) primary productivity simulated in their model and the preservation of organic-rich
372 (organic-poor) sediments in the geological record of the late Katian (i.e., the first time slice of
373 Melchin *et al.* 2013). Similar to the cherts and phosphate deposits of Pope & Steffen (2003), the black
374 shales are documented on the western margins of equatorial Laurentia and equatorial Gondwana,
375 thus matching simulated upwelling systems (Fig. 1A). More interestingly, the deposits depleted in
376 organic matter are found around Baltica and along the coast of Gondwana over the South Pole
377 (Melchin *et al.* 2013), precisely where the model simulates local NPP minima (Fig. 1A). This model-
378 data agreement supports the spatial patterns of NPP simulated in the present study. It also suggests
379 that the preservation of black shales in the late Katian may have been driven by the patterns of
380 primary production at the ocean surface (Pohl *et al.* 2017).

381 Baltoscandian reefs and mounds

382 In their comprehensive review, Kröger *et al.* (2016) demonstrated a critical change in the mode of
383 carbonate production across the Baltic Basin during the latest Sandbian – earliest Katian (Late
384 Ordovician, ca. 453 Ma). This boundary marked the beginning of a protracted period of widespread
385 development of reefs in shallow-water areas and mud mounds in deeper epicontinental settings. The
386 authors showed that biotic factors do not explain the initiation of Late Ordovician bioherm growth.
387 They postulated climatic and eustatic drivers and further identified the northward drift of Baltica as
388 the main determining factor for the timing of the start of the Baltic reef and mound development.
389 More specifically, they suggested that *‘the entry of Baltica in a geographical zone that allowed for a*
390 *widespread bioherm formation was a major factor for the Sandbian radiation of reefal and reef-*
391 *related organisms’*. Although the most direct effect of the latitudinal shift of Baltica was probably the
392 establishment of climatic conditions more favourable to the shallow-water carbonate factory, our
393 model runs also indicate that this northward migration made Baltica enter the nutrient-depleted
394 tropical region during the Late Ordovician (Fig. 1A). Such unparalleled oligotrophic conditions may
395 have provided the appropriate environmental background for the explosion of the bioherms on
396 Baltoscandia.

397

398 **Limitations**

399 Our simulations provide an overview of possible spatial patterns of Ordovician NPP in time and space.
400 However, it does not tell us anything about the total amount of NPP. The latter is a relatively direct
401 function of nutrient availability in the ocean, which depends in turn on the intensity of continental
402 weathering. Estimating continental weathering requires major assumptions on both the lithology and
403 vegetation cover of emerged continental masses and global climate (e.g. Godd ris *et al.* 2014). In
404 particular, weathering may have significantly varied throughout the Ordovician as a result of changes
405 in global climate (Trotter *et al.* 2008), continental configuration (Nardin *et al.* 2011), volcanic activity
406 (Lefebvre *et al.* 2010), land-ice cover (Pogge von Strandmann *et al.* 2017) or in response to the
407 advent of the first land plants (Lenton *et al.* 2012; 2016; Porada *et al.* 2016). Such mechanisms do lie
408 beyond what we are able to resolve using our ocean-atmosphere model. As a result, we are unable
409 to predict the trend towards an increase or a decrease in NPP throughout the period.

410

411 **Conclusion**

412 Numerical simulations conducted with an ocean-atmosphere general circulation model with
413 biogeochemical capabilities (MITgcm) predict the position and longevity of upwelling zones in the
414 Ordovician Earth system. Upwelling zones host specific types of ecosystems, characterised by high
415 organic productivity, abundant organisms (commonly opportunist species, often soft-bodied) but not
416 necessarily high diversities. Nevertheless, high productivity levels may have provided the primary
417 resources needed by superior consumers and thus paved the way for the development of more
418 complex trophic chains featuring more diverse taxonomic assemblages. Fossil data have, to date, not
419 been aligned with these predictions although accumulations of organic matter, bone and skeletal
420 concentrations are identifiable in the fossil record and can be correlated with characteristic
421 sediments, such as cherts, that signpost upwelling zones in deep time. The present study therefore
422 targets in-depth analysis of the smaller members of the fossil record as the logical next step towards
423 the integrated understanding of the diversification patterns throughout the early Palaeozoic.

424

425 **Acknowledgments**

426 The findings in this study are based on climatic fields simulated by the ocean-atmosphere general
427 circulation model MITgcm. Code for the climate model MITgcm can be accessed at <http://mitgcm.org>.
428 Requests for the climate model output can be sent to A.P (pohl@cerege.fr). The authors thank Peter

429 Doyle and Alan Owen for editorial handling. We also thank Tom Challands and Axel Munnecke for
430 helpful and constructive reviews, and the guest-editors of this volume for the invitation to submit.
431 The authors acknowledge the financial support from the CNRS (INSU, action SYSTER). A.P. and Y.D.
432 thank the CEA/CCRT for providing access to the HPC resources of TGCC under the allocation 2014-
433 012212 made by GENCI. A.P. thanks Maura Brunetti from the University of Geneva and David
434 Ferreira from the University of Reading, who provided expertise that greatly assisted the research.
435 This research was funded through a CEA PhD grant CFR. This is a contribution to the IGCP Project-653,
436 'The onset of the Great Ordovician Biodiversification Event'. D.A.T.H. acknowledges financial support
437 from the Leverhulme Trust and the Wenner Gren Foundation.

438

439

440 **References**

- 441 Adcroft, A., Campin, J.M. and Hill, C. 2004: Implementation of an atmosphere-ocean general
442 circulation model on the expanded spherical cube. *Monthly Weather Review* 132, 2845–2863.
- 443 Allmon, W.D. and Martin, R.E. 2014. Seafood through time revisited: the Phanerozoic increase in
444 marine trophic resources and its macroevolutionary consequences. *Paleobiology* 40, 256–287.
- 445 Alroy, J. 2010: The shifting balance of diversity among major marine animal groups. *Science* 329,
446 1191–1194.
- 447 Arntz, W.E., Gallardo, V.A., D. Gutiérrez, D., Isla, E., Levin, L.A., Mendo, J., Neira, C., Rowe, G.T.,
448 Tarazona, J. and Wolff, M. 2006. El Niño and similar perturbation effects on the benthos of the
449 Humboldt, California, and Benguela Current upwelling ecosystems. *Advances in Geosciences* 6,
450 243–265.
- 451 Bambach, R. K., 2006: Phanerozoic Biodiversity Mass Extinctions. *The Annual Review of Earth and*
452 *Planetary Science* 34, 127–155.
- 453 Berner, R.A. 2006: GEOCARBSULF: A combined model for Phanerozoic atmospheric O₂ and CO₂.
454 *Geochimica et Cosmochimica Acta* 70, 5653–5664.
- 455 Brunetti, M., Vérard, C. and Baumgartner, P.O. 2015: Modeling the Middle Jurassic ocean circulation.
456 *Journal of Palaeogeography* 4, 371–383.
- 457 Bryant, R.G. 2013: Recent advances in our understanding of dust source emission processes. *Progress*
458 *in Physical Geography* 37, 397–421.
- 459 Buitenhuis, E.T., Li, W.K.W., Lomas, M.W., Karl, D.M., Landry, M.R, Jacquet, S., 2012: Picoheterotroph
460 (Bacteria and Archaea) biomass distribution in the global ocean. *Earth System Science Data* 4,
461 101–106.
- 462 Buitenhuis, E.T., Vogt, M., Moriarty, R., Bednarsek, N., Doney, S.C., Leblanc, K., Le Quéror, C., Luo, Y.-
463 W., O'Brien, C., O'Brien, T., Peloquin, J., Schiebel, R., Swan, C., 2013: MAREDAT: towards a world
464 atlas of MARine Ecosystem DATa. *Earth System Science Data* 5, 227–239.
- 465 Christiansen, J.L. & Stouge, S., 1999: Oceanic circulation as an element in palaeogeographical
466 reconstructions: the Arenig (early Ordovician) as an example. *Terra Nova* 11, 73–78
- 467 Cocks, L.R.M. and Torsvik, T.H. 2005: Baltica from the late Precambrian to mid-Palaeozoic times: The
468 gain and loss of a terrane's identity. *Earth-Science Reviews* 72, 39–66.
- 469 Cocks, L.R.M. and Torsvik, T.H. 2007: Siberia, the wandering northern terrane, and its changing
470 geography through the Palaeozoic. *Earth-Science Reviews* 82, 29–74.
- 471 Cocks, L.R.M. and Torsvik, T.H. 2011: The Palaeozoic geography of Laurentia and western Laurussia: A

472 stable craton with mobile margins. *Earth-Science Reviews* 106, 1–51.

473 Cocks, L.R.M. and Torsvik, T.H. 2013: The dynamic evolution of the Palaeozoic geography of eastern
474 Asia. *Earth-Science Reviews* 117, 40–79.

475 de Vargas, C., Audic, S., Henry, N., Decelle, J., Mahe, F., Logares, R., Lara, E., Berney, C., Le Bescot, N.,
476 Probert, I., Carmichael, M., Poulain, J., Romac, S., Colin, S., Aury, J.M., Bittner, L., Chaffron, S.,
477 Dunthorn, M., Engelen, S., Flegontova, O., Guidi, L., Horak, A., Jaillon, O., Lima-Mendez, G., Luke,
478 J., Malviya, S., Morard, R., Mulot, M., Scalco, E., Siano, R., Vincent, F., Zingone, A., Dimier, C.,
479 Picheral, M., Searson, S., Kandels-Lewis, S., Tara Oceans Coordinators, Acinas, S.G., Bork, P.,
480 Bowler, C., Gorsky, G., Grimsley, N., Hingamp, P., Iudicone, D., Not, F., Ogata, H., Pesant, S., Raes,
481 J., Sieracki, M.E., Speich, S., Stemmann, L., Sunagawa, S., Weissenbach, J., Wincker, P., Karsenti,
482 E., Boss, E., Follows, M., Karp-Boss, L., Krzic, U., Reynaud, E.G., Sardet, C., Sullivan, M.B. and
483 Velayoudon, D. 2015: Eukaryotic plankton diversity in the sunlit ocean. *Science* 348, 1261605–
484 1261605.

485 Dutkiewicz, S., Follows, M.J. and Parekh, P. 2005: Interactions of the iron and phosphorus cycles: A
486 three-dimensional model study. *Global Biogeochemical Cycles* 19, GB1021.

487 Edwards, D., Cherns, L. and Raven, J.A. 2015: Could land-based early photosynthesizing ecosystems
488 have bioengineered the planet in mid-Palaeozoic times? *Palaeontology* 58, 803–837.

489 Eisenbarth, S. and Zettler, M.L. 2016. Diversity of the benthic macrofauna off northern Namibia from
490 the shelf to the deep sea. *Journal of Marine Systems* 155, 1–10.

491 Enderton, D. and Marshall, J. 2009: Explorations of atmosphere–ocean–ice climates on an
492 aquaplanet and their meridional energy transports. *Journal of the Atmospheric Sciences* 66,
493 1593–1611.

494 Falkowski, P. 2012: Ocean science: the power of plankton. *Nature* 483, S17–S20.

495 Ferreira, D., Marshall, J. and Campin, J.-M. 2010: Localization of deep water formation: role of
496 atmospheric moisture transport and geometrical constraints on ocean circulation. *Journal of*
497 *Climate* 23, 1456–1476.

498 Ferreira, D., Marshall, J. and Rose, B. 2011: Climate determinism revisited: multiple equilibria in a
499 complex climate model. *Journal of Climate* 24, 992–1012.

500 Finnegan, S. and Droser, M.L. 2005. Relative and absolute abundance of trilobites and
501 rhynchonelliform brachiopods across the Lower/Middle Ordovician Boundary, Eastern Basin and
502 Range. *Paleobiology* 31, 480-502.

503 Finnegan, S. and Droser, M.L. 2008: Body size, energetics, and the Ordovician restructuring of marine
504 ecosystems. *Paleobiology* 34, 342–359.

505 Finney, S.C., Berry, W.B.N. and Cooper, J.D. 2007. The influence of denitrifying seawater on graptolite
506 extinction and diversification during the Hirnantian (latest Ordovician) mass extinction event.
507 *Lethaia* 40, 281-291.

508 Franck, S., Bounama, C. and Bloh, Von, W. 2006: Causes and timing of future biosphere extinctions.
509 *Biogeosciences* 3, 85–92.

510 Friis, K., Najjar, R.G., Follows, M.J. and Dutkiewicz, S. 2006: Possible overestimation of shallow-depth
511 calcium carbonate dissolution in the ocean. *Global Biogeochemical Cycles* 20, GB4019.

512 Friis, K., Najjar, R.G., Follows, M.J., Dutkiewicz, S., Körtzinger, A. and Johnson, M. 2007: Dissolution of
513 calcium carbonate: observations and model results in the subpolar North Atlantic.
514 *Biogeosciences* 4, 205–213.

515 Gent, P.R. and McWilliams, J.C. 1990: Isopycnal mixing in ocean circulation models. *Journal of*
516 *Physical Oceanography* 20, 150–155.

517 Goddérís, Y., Donnadieu, Y., Le Hir, G., Lefebvre, V. and Nardin, E. 2014: The role of palaeogeography
518 in the Phanerozoic history of atmospheric CO₂ and climate. *Earth-Science Reviews* 128, 122–138.

519 Harper, D.A.T. 2006: The Ordovician biodiversification: Setting an agenda for marine life.
520 *Palaeogeography, Palaeoclimatology, Palaeoecology* 232, 148-166.

521 Harper, D.A.T., Hammarlund, E.U. and Rasmussen, C.M.Ø. 2014. End Ordovician extinctions: A
522 coincidence of causes. *Gondwanan Research* 25, 1294–1307.

523 Harper, D.A.T., Zhan, R.-B. and Jin, J. 2015: The Great Ordovician Biodiversification Event: Reviewing

524 two decades of research on diversity's big bang illustrated by mainly brachiopod data.
525 *Palaeoworld* 24, 75–85.

526 Herrmann, A.D., Haupt, B.J., Patzkowsky, M.E., Seidov, D. and Slingerland, R.L. 2004: Response of
527 Late Ordovician paleoceanography to changes in sea level, continental drift, and atmospheric
528 $p\text{CO}_2$: potential causes for long-term cooling and glaciation. *Palaeogeography,*
529 *palaeoclimatology, palaeoecology* 210, 385–401.

530 Irigoien, X., Huisman, J. and Harris, R.P. 2004: Global biodiversity patterns of marine phytoplankton
531 and zooplankton. *Nature* 429, 863–867.

532 Kallmeyer, J., Pockalny, R., Adhikari, R.R., Smith, D.C. and D'Hondt, S. 2012: Global distribution of
533 microbial abundance and biomass in subseafloor sediment. *109*, 16213–16216.

534 Kröger, B., Hints, L. and Lehnert, O. 2016: Ordovician reef and mound evolution: the Baltoscandian
535 picture. *Geological Magazine*, 1–24.

536 Large, W.G., McWilliams, J.C. and Doney, S.C. 1994: Oceanic vertical mixing: a review and a model
537 with a nonlocal boundary layer parameterization. *Reviews of Geophysics* 32, 363–403.

538 Lees, D.C., Fortey, R.A. and Cocks, L.R.M. 2002: Quantifying paleogeography using biogeography: a
539 test case for the Ordovician and Silurian of Avalonia based on brachiopods and trilobites.
540 *Paleobiology* 28, 343–363.

541 Lefebvre, V., Servais, T., François, L. and Averbuch, O. 2010: Did a Katian large igneous province
542 trigger the Late Ordovician glaciation? A hypothesis tested with a carbon cycle model.
543 *Palaeogeography, palaeoclimatology, palaeoecology* 296, 310–319.

544 Lenton, T.M., Crouch, M., Johnson, M., Pires, N. and Dolan, L. 2012: First plants cooled the
545 Ordovician. *Nature Geoscience* 5, 86–89.

546 Lenton, T.M., Dahl, T.W., Daines, S.J., Mills, B.J.W., Ozaki, K., Saltzman, M.R. and Porada, P. 2016:
547 Earliest land plants created modern levels of atmospheric oxygen. *Proceedings of the National*
548 *Academy of Sciences of the United States of America*, 201604787.

549 Leslie, S.A. and Bergström, S.M. 2003. Widespread, prolonged late Middle to Late Ordovician
550 upwelling in North America: A proxy record of glaciation?: Comment and Reply. *Geology* 31, e28-
551 e29.

552 Levin, L.A. 2003. Oxygen minimum zone benthos: adaptation and community response to hypoxia.
553 *Oceanography and Marine Biology: an Annual Review* 41, 1–45.

554 Marshall, J., Adcroft, A., Campin, J.M., Hill, C. and White, A. 2004: Atmosphere-ocean modeling
555 exploiting fluid isomorphisms. *Monthly Weather Review* 132, 2882–2894.

556 Marshall, J., Adcroft, A., Hill, C., Perelman, L. and Heisey, C. 1997a: A finite-volume, incompressible
557 Navier Stokes model for studies of the ocean on parallel computers. *Journal of Geophysical*
558 *Research* 102, 5753–5766.

559 Marshall, J., Hill, C., Perelman, L. and Adcroft, A. 1997b: Hydrostatic, quasi-hydrostatic, and
560 nonhydrostatic ocean modeling. *Journal of Geophysical Research* 102, 5733–5752.

561 Martin, J.H., Knauer, G.A., Karl, D.M. and Broenkow, W.W. 1987: VERTEX: carbon cycling in the
562 northeast Pacific. *Deep Sea Research* 34, 267–285.

563 Martin, R.E., 2003: The fossil record of biodiversity: nutrients, productivity, habitat area and
564 differential preservation. *Lethaia* 36, 179-193.

565 Martin, R.E., Quigg, A., Podkovyrov, V., 2008: Marine biodiversification in response to evolving
566 phytoplankton stoichiometry. *Palaeogeography, Palaeoclimatology, Palaeoecology* 258, 277-291

567 Melchin, M.J., Mitchell, C.E., Holmden, C., & Štorch, P., 2013. Environmental changes in the Late
568 Ordovician-early Silurian: Review and new insights from black shales and nitrogen isotopes.
569 *Geological Society of America Bulletin*, 125(11-12), 1635–1670.

570 Molteni, F. 2003: Atmospheric simulations using a GCM with simplified physical parametrizations. I:
571 Model climatology and variability in multi-decadal experiments. *Climate Dynamics* 20, 175–191.

572 Montenegro, A., Spence, P., Meissner, K.J., Eby, M., Melchin, M.J. and Johnston, S.T. 2011: Climate
573 simulations of the Permian-Triassic boundary: Ocean acidification and the extinction event.
574 *Paleoceanography* 26, PA3207.

575 Moriarty, R., O'Brien, T.D., 2013: Distribution of mesozooplankton biomass in the global ocean. *Earth*

576 *System Science Data* 5, 45-55.

577 Nardin, E., Godd ris, Y., Donnadieu, Y., Le Hir, G., Blakey, R.C., Puc at, E. and Aretz, M. 2011:

578 Modeling the early Paleozoic long-term climatic trend. *Geological Society of America Bulletin*

579 *123*, 1181–1192.

580 Nowak, H., Servais, T., Monnet, C., Molyneux, S.G., Vandenbroucke, T.R.A., 2015. Phytoplankton

581 dynamics from the Cambrian Explosion to the onset of the Great Ordovician Biodiversification

582 Event: a review of Cambrian acritarch diversity. *Earth-Science Reviews* 151, 117–131.

583 Osen, A.K., Winguth, A.M.E., Winguth, C. and Scotese, C.R. 2012: Sensitivity of Late Permian climate

584 to bathymetric features and implications for the mass extinction. *Global and Planetary Change*,

585 171–179.

586 Payne, J.L. and Finnegan, S. 2006: Controls on marine animal biomass through geological time.

587 *Geobiology* 4, 1-10.

588 Pogge von Strandmann, P.A.E., Desrochers, A., Murphy, M.J., Finlay, A.J., Selby, D. and Lenton, T.M.

589 2017: Global climate stabilisation by chemical weathering during the Hirnantian glaciation.

590 *Geochemical Perspectives Letters*, 230–237.

591 Pohl, A., Donnadieu, Y., Le Hir, G., Buoncristiani, J.F. and Vennin, E. 2014: Effect of the Ordovician

592 paleogeography on the (in)stability of the climate. *Climate of the Past* 10, 2053–2066.

593 Pohl, A., Donnadieu, Y., Le Hir, G., & Ferreira, D. 2017. The climatic significance of Late Ordovician-

594 early Silurian black shales. *Paleoceanography*, 32(4), 397–423.

595 Pohl, A., Donnadieu, Y., Le Hir, G., Ladant, J.B., Dumas, C., Alvarez-Solas, J. and Vandenbroucke, T.R.A.

596 2016a: Glacial onset predated Late Ordovician climate cooling. *Paleoceanography* 31, 800–821.

597 Pohl, A., Nardin, E., Vandenbroucke, T. and Donnadieu, Y. 2016b: High dependence of Ordovician

598 ocean surface circulation on atmospheric CO₂ levels. *Palaeogeography, palaeoclimatology,*

599 *palaeoecology* 458, 39–51.

600 Pope, M.C. and Steffen, J.B. 2003: Widespread, prolonged late Middle to Late Ordovician upwelling in

601 North America: A proxy record of glaciation? *Geology* 31, 63–66.

602 Porada, P., Lenton, T.M., Pohl, A., Weber, B., Mander, L., Donnadieu, Y., Beer, C., P schl, U. and

603 Kleidon, A. 2016: High potential for weathering and climate effects of non-vascular vegetation in

604 the Late Ordovician. *Nature communications* 7, 12113.

605 Poussart, P.F., Weaver, A.J. and Barnes, C.R. 1999: Late Ordovician glaciation under high atmospheric

606 CO₂: A coupled model analysis. *Paleoceanography* 14, 542–558.

607 Pruss, S.B., Finnegan, S., Fischer, W.W. and Knoll, A.H. 2010. Carbonates in skeleton-poor seas: new

608 insights from Cambrian and Ordovician strata of Laurentia. *Palaios* 25, 73-84.

609 Redi, M.H. 1982: Oceanic isopycnal mixing by coordinate rotation. *Journal of Physical Oceanography*

610 *12*, 1154–1158.

611 Rosenberg, R., Arntz, W. E., Chuman de Flores, E., Flores, L. A., Carbajal, G., Finger, G. & Tarazona, J.

612 1983. Benthos biomass and oxygen deficiency in the upwelling system off Peru. *Journal of*

613 *Marine Research* 41, 263–279.

614 Rubinstein, C.V., Gerrienne, P., la Puente, de, G.S., Astini, R.A. and Steemans, P. 2010: Early Middle

615 Ordovician evidence for land plants in Argentina (eastern Gondwana). *New Phytologist* 188,

616 365–369.

617 Ruttenberg, K.C. 1993: Reassessment of the oceanic residence time of phosphorus. *Chemical Geology*

618 *107*, 405–409.

619 Saltzman, M.R., Young, S.A. and Kump, L.R. 2011: Pulse of atmospheric oxygen during the late

620 Cambrian.

621 Sepkoski, J.J., Jr. 1995. The Ordovician Radiations: Diversification and extinction shown by global

622 genus level taxonomic data; pp. 393–396 in J. D. Cooper, M. L. Droser, and S. C. Finney (eds.),

623 Ordovician Odyssey: Short Papers, 7th International Symposium on the Ordovician System. Book

624 77, Pacific Section Society for Sedimentary Geology (SEPM), Fullerton, California.

625 Sepkoski, J.J., Bambach, R.K., Raup, D.M. and Valentine, J.W. 1981: Phanerozoic marine diversity and

626 the fossil record. *Nature* 293, 435–437.

627 Servais, T., Lehnert, O., Li, J., Mullins, G.L., Munnecke, A., N tzel, A., Vecoli, M. 2008: The Ordovician

628 Biodiversification: revolution in the oceanic trophic chain. *Lethaia* 41, 99–109.

629 Servais, T., Harper, D. A. T., Li, J., Munnecke, A., Owen, A. W., Sheehan, P. M. 2009: Understanding
630 the Great Ordovician Biodiversification Event (GOBE): Influences of paleogeography,
631 paleoclimate, or paleoecology? *GSA Today* 19 (4/5).

632 Servais, T., Owen, A.W., Harper, D.A.T., Kröger, B., Munnecke, A. 2010: The Great Ordovician
633 Biodiversification Event (GOBE): the palaeoecological dimension. *Palaeogeography,*
634 *Palaeoclimatology, Palaeoecology* 294, 99-119.

635 Servais, T., Danelian, T., Harper, D.A.T., Munnecke, A. 2014: Possible oceanic circulation patterns,
636 surface water currents and upwelling zones in the Early Palaeozoic. *GFF* 136, 229-233.

637 Servais, T., Perrier, V., Danelian, T., Klug, C., Martin, R., Munnecke, A., Nowak, H., Nützel, A.,
638 Vandenbroucke, T. R. A., Williams, M. Rasmussen, C. M. Ø. 2016: The onset of the ‘Ordovician
639 Plankton Revolution’ in the late Cambrian. *Palaeogeography, Palaeoclimatology, Palaeoecology*
640 458, 12-28.

641 Sigman, D.M. and Hain, M.P. 2012: The Biological Productivity of the Ocean. *Nature Education* 3, 1-
642 16.

643 Stanley, S.M., 2016. Estimates of the magnitudes of major marine mass extinctions in earth history.
644 *Proceedings National Academy of Sciences* 113, 6325-6334.

645 Taylor, P.D. and Sendino, C. 2010. Latitudinal distribution of bryozoan-rich sediments in the
646 Ordovician. *Bulletin of Geosciences* 85, 565–572.

647 Thiel, H. 1982. Zoobenthos of the CINECA area and other upwelling regions. *Rapp. P.-v. Réunion. Cons.*
648 *Int. Explor. Mer.* 180, 323-334.

649 Torsvik, T.H. and Cocks, L.R.M. 2009: *BugPlates: linking biogeography and palaeogeography,*
650 *software manual.* geodynamics.no. Downloaded from <http://www.geodynamics.no> on 30 July
651 2014.

652 Torsvik, T.H. and Cocks, L.R.M. 2013: Gondwana from top to base in space and time. *Gondwana*
653 *Research* 24, 999–1030.

654 Trotter, J.A., Williams, I.S., Barnes, C.R., Lécuyer, C. and Nicoll, R.S. 2008: Did cooling oceans trigger
655 Ordovician biodiversification? Evidence from conodont thermometry. *Science* 321, 550–554.

656 Wallmann, K. 2003: Feedbacks between oceanic redox states and marine productivity: A model
657 perspective focused on benthic phosphorus cycling. *Global Biogeochemical Cycles* 17, 1084.

658 Webby, B.D. 2004. Introduction. In: Webby, B.D., Paris, F., Droser, M.L., Percival I.G. (Eds.), *The Great*
659 *Ordovician Biodiversification Event.* Columbia University Press, New York, pp. 1-37.

660 Webby, B.D., Paris, F., Droser, M.L. and Percival I.G. (Eds.), *The Great Ordovician Biodiversification*
661 *Event.* Columbia University Press, New York

662 Wilde, P. 1991: Oceanography in the Ordovician. In Barnes, C. R., Williams, S. H. (eds.), *Advances in*
663 *Ordovician Geology, Vol. 90,* 283–298. Geological Survey of Canada.

664 Winton, M. 2000: A reformulated three-layer sea ice model. *Journal of Atmospheric and Oceanic*
665 *Technology* 17, 525–531.

666

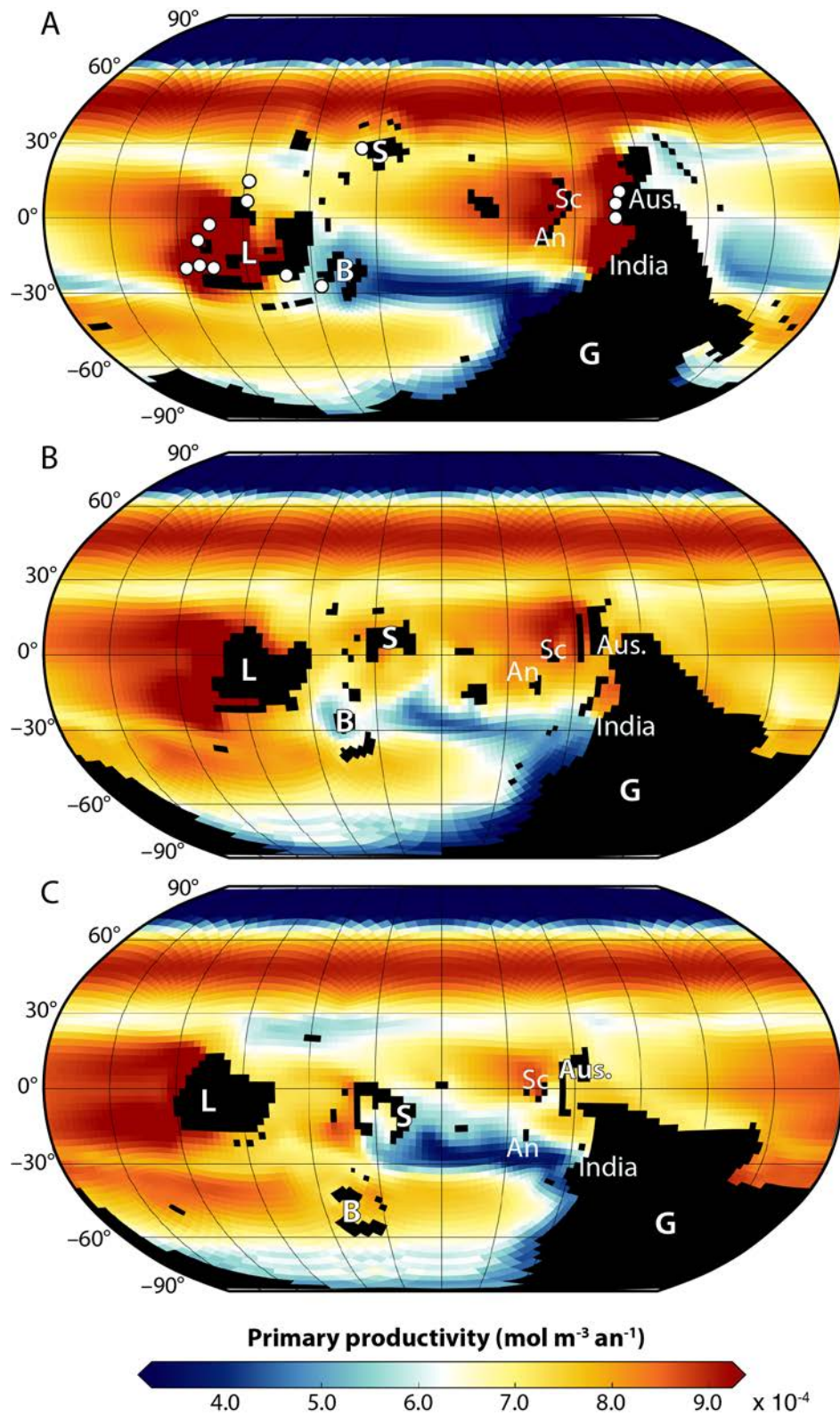


Figure 1: Surface primary productivity simulated at 440 Ma (A), 460 Ma (B) and 480 Ma (C). The black mask indicates continental masses. In subfigure A, white points represent

evidence of upwelling. The latter are plotted on the Late Ordovician time slice following Pope & Steffen (2003), but see discussion in the main text. *L: Laurentia; B: Baltica; S: Siberia; G: Gondwana; Sc: South China; An: Annamia; Aus: Australia.*